



Application Notes

High-Selectivity Microstrip Filters Based on Structures With a Limited Number of Hairpin Resonators

■ Grigory M. Aristarkhov, Andrei Grebennikov, and Nikita V. Zvezdinov

Microstrip filters on half-wave hairpin resonators are widely used in different microwave applications because they are very compact structures and do not contain short circuit elements, characteristics that make them relatively easy to manufacture and use over a wide frequency range. In this class of microstrip filters, three basic structures can be defined: one based on hairpin resonators with alternating orientations [Figure 1(a)], another based on codirectional hairpin resonators [Figure 1(b)], and a third based on filters using hairpin resonators with supplementary electromagnetic couplings between nonadjacent resonators [Figure 1(c)]. These structures are fundamentally different both in their operating principles and in their achievable characteristics despite layouts that, for two of them, seem similar.

Grigory M. Aristarkhov (g.aristarkhov2010@yandex.ru) and Nikita V. Zvezdinov are with Moscow Technical University of Communications and Informatics, Russia. Andrei Grebennikov (grandrei@ieee.org) is with Sumitomo Electric Europe, Elstree, United Kingdom.

*Digital Object Identifier 10.1109/MMM.2019.2935362
Date of current version: 11 October 2019*



ISTOCKPHOTO.COM/OLGASALT

Among these three basic filter structures, microstrip filters based on hairpin resonators with alternating orientations are characterized by the lowest frequency selectivity. The basic elements of such structures use multiple coupled quarter-wave microstrip lines with diagonal connections that limit the number of attenuation poles close to the filter passband [1]. The formation of attenuation poles close to the filter passband can be achieved using the coupling

between nonadjacent resonators [2]–[4], a dual-plane filter structure based on conductor-backed coplanar waveguides [5], a quasi-hairpin filter based on separated coupling paths [6], a cross-coupled wiggly-line hairpin resonator filter [7], or a third-order hairpin filter with weak signal-interference coupling between the input and output nodes [8]. By optimizing the supplementary magnetic and electrical couplings in an N -resonator microstrip structure, it is possible to form $(N - 2)$ attenuation poles at certain frequencies close to the passband. For example, in a four-resonator microstrip filter structure similar to that shown in Figure 1(c), only two attenuation poles can be created [9].

The operating principle of microstrip filters with codirectional hairpin resonators is based on nonequal

even- and odd-mode wave velocities in an inhomogeneous dielectric structure for pairs of coupled microstrip lines when it is potentially possible to form $(N + 1)$ attenuation poles at certain frequencies close to the passband without creating any special couplings between nonadjacent resonators [10], [11]. In these microstrip filters with codirectional hairpin resonators, the attenuation pole typically occurs below the passband. The position of this attenuation pole can be controlled by the addition of capacitive coupling between the open ends of adjacent resonators when the attenuation poles move upward in frequency and cause the passband to narrow [12].

The potential high-selectivity capability of these structures is limited because the number of created attenuation poles does not usually exceed the number of nonadjacent resonators in a microstrip bandpass-filter structure. Therefore, an improvement of the selectivity properties of these microstrip filters can be achieved only by using more resonators. Because of the limited quality factor of the microstrip resonators, a substantial increase in their numbers will result in a significant increase in the passband insertion loss and overall filter size, without any improvement in the filter roll-off factor.

This limitation becomes problematic when sufficiently thin dielectric substrates with thicknesses $H \leq 0.25$ mm are used. Such substrates are widely employed to prevent the excitation of higher-type waves in microstrip structures intended for use at high microwave and millimeter-wave frequencies and to minimize the overall circuit size. They are also used in monolithic microwave integrated circuits. When used in such circuits, the quality factor of microstrip resonators declines. As a result, the frequency-selectivity limit of the microstrip bandpass filter will occur with a substantially lower number of resonators, typically $N \leq 4$.

This raises an important question: Is it possible to increase the number of attenuation poles in a microstrip bandpass filter while simultaneously decreasing the number of resonators close to their limited number when the filter structure contains no more than two to four resonators? This is possible only when the basic filter two-resonator structure has the properties of the multiresonant microwave circuit.

Nontraditional microstrip bandpass-filter structures with a limited number of codirectional hairpin resonators are capable of forming a significant number of attenuation poles at certain frequencies, often exceeding the number of resonators in a filter structure. This provides a much higher frequency selectivity of the microstrip bandpass filter by combining different wave properties of the microstrip lines and different design methods to control the wave processes in them.

Two-Resonator Structures and Their Operation Principle

The basic structure of a two-resonator microstrip filter is represented by two electromagnetically coupled half-wave codirectional hairpin units. The topology of this structure is shown in Figure 2(b) with the corresponding cross section in Figure 2(a), where W is the width of the microstrip line, S is the spacing between the microstrip lines, H is the substrate thickness, and ϵ_r is the effective dielectric permittivity. The basic two-resonator filter structure is composed of a central two-line lattice section [Figure 2(c)] and two

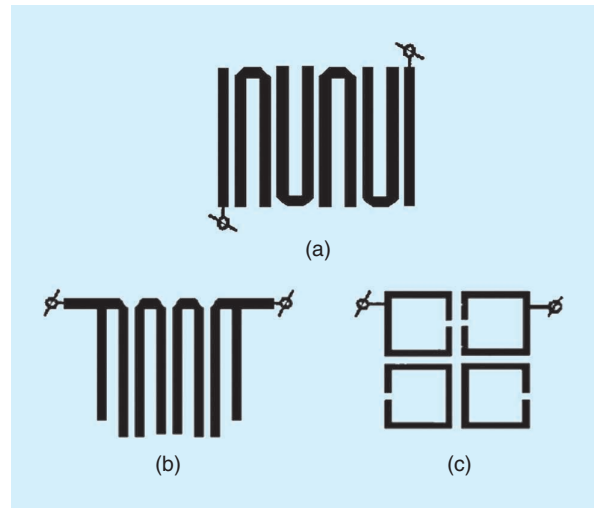


Figure 1. The basic structures of microstrip filters based on (a) hairpin resonators with alternating orientations, (b) codirectional hairpin resonators, and (c) filters using hairpin resonators with supplementary electromagnetic couplings between nonadjacent resonators.

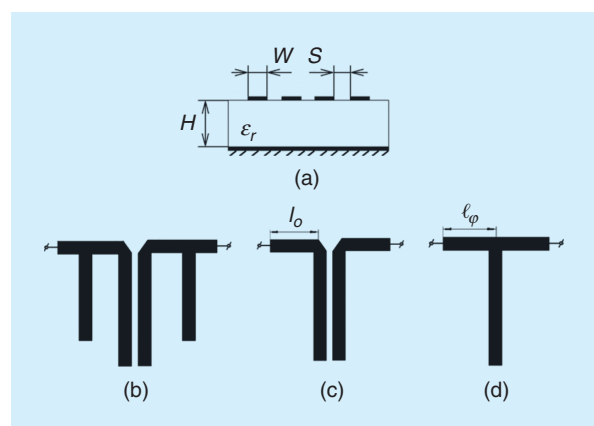


Figure 2. A two-resonator microstrip filter and its elements. (a) A cross section and (b) the topology of the structure corresponding to (a). The basic two-resonator filter structure is composed of (c) a central two-line lattice section and two K inverters implemented in the form of (d) a T-type, open-stub microstrip section.

K inverters implemented in the form of a T-type, open-stub microstrip section [Figure 2(d)]. The frequency properties of these two-resonator microstrip filters can be investigated based on the distribution of the attenuation poles of the filter amplitude response along the frequency axis.

To define the frequency properties of a two-resonator microstrip filter, first consider the formation of the amplitude response of a codirectional quarter-wave lattice unit. Figure 3 shows a step-by-step process for the equivalent transformation of such a quarter-wave lattice section into a fully balanced bridge-type structure in the form of an equivalent-mode representation using the method of mirror images [13]. In this equivalent-mode representation, each normal (even and odd mode) wave propagated in a system of two coupled microstrip lines corresponds to its own resonator with wave parameters according to the corresponding type of excitation in a system of two coupled lines.

In the case of an inhomogeneous, lossless coupled-line structure, the four-port impedance Z matrix for a single lattice section [Figure 3(a)] can be written as

$$[Z] = \frac{1}{2} \begin{bmatrix} Z_b + Z_a & Z_b - Z_a \\ Z_b - Z_a & Z_b + Z_a \end{bmatrix}, \quad (1)$$

where Z_a is the impedance of the series two-terminal network [Figure 3(b)], defined as the input impedance of the original two-port network under its odd-mode excitation,

$$Z_a = jX_a = -jZ_{0o} \cot \theta_{0o} = -jZ_{0o} \cot \left(\frac{\pi}{2} \frac{f}{f_{0o}} \right), \quad (2)$$

and Z_b is the impedance of the diagonal two-terminal network [Figure 3(b)], defined as the input impedance of the original two-port network under its even-mode excitation,

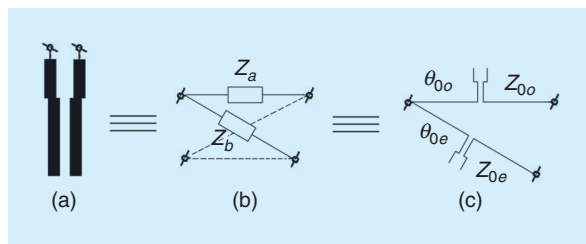


Figure 3. The equivalent-mode representation of the lattice section. (a) A single lattice section. (b) An illustration showing that Z_a is the impedance of the series two-terminal network and Z_b is the impedance of the diagonal two-port network. (c) An illustration showing that Z_{0e} and Z_{0o} are the even- and odd-mode characteristic impedances and that θ_{0e} and θ_{0o} are the even- and odd-mode electrical lengths of a system of two coupled transmission lines.

$$Z_b = jX_b = -jZ_{0e} \cot \theta_{0e} = -jZ_{0e} \cot \left(\frac{\pi}{2} \frac{f}{f_{0e}} \right), \quad (3)$$

where Z_{0e} and Z_{0o} are the even- and odd-mode characteristic impedances, θ_{0e} and θ_{0o} , are the even- and odd-mode electrical lengths of a system of two coupled transmission lines [Figure 3(c)], and f_{0e} and f_{0o} are the frequencies at which the lattice section is a quarter-wavelength long electrically under even and odd excitation modes, respectively [13].

The resonant frequencies of a quarter-wave section of length l defined from conditions $X_a(f_{0o}) = 0$ and $X_b(f_{0e}) = 0$ are equal and written as

$$f_{0e} = f_b = \frac{v_{0e}}{4l} = \frac{c}{\sqrt{\epsilon_{0e}} 4l}, \quad (4)$$

and

$$f_{0o} = f_a = \frac{v_{0o}}{4l} = \frac{c}{\sqrt{\epsilon_{0o}} 4l}, \quad (5)$$

where c is the speed of light in a vacuum, v_{0e} and v_{0o} are the phase velocities of the even- and odd-mode waves, and ϵ_{0e} and ϵ_{0o} are the effective dielectric permittivities of a system of two coupled microstrip lines under even and odd excitation modes, respectively.

In this case, the coefficients of a magnetic (inductive) coupling K_L and an electrical (capacitive) coupling K_C in a system of two coupled microstrip lines can be defined through the wave parameters as

$$K_L = \frac{Z_{0e} - Z_{0o} \sqrt{\epsilon_{0o}/\epsilon_{0e}}}{Z_{0e} + Z_{0o} \sqrt{\epsilon_{0o}/\epsilon_{0e}}} \quad (6)$$

and

$$K_C = \frac{Z_{0e} - Z_{0o} \sqrt{\epsilon_{0e}/\epsilon_{0o}}}{Z_{0e} + Z_{0o} \sqrt{\epsilon_{0e}/\epsilon_{0o}}}. \quad (7)$$

From (6) and (7) it follows that $K_L = K_C = K$ under the condition of the phase synchronization of the even- and odd-mode waves when $v_{0e} = v_{0o}$ and $f_a = f_{0o} = f_{0e} = f_b$, thus resulting in degeneration of the characteristic passband $\Delta f_c = |f_a - f_b| = 0$, where the image impedance of the equivalent two-port network $Z_c = \sqrt{-X_a X_b}$ is real. The lattice section represents an all-stop circuit under the condition of the phase synchronization, for example, in a homogeneous dielectric medium where the electrical lengths for even and odd modes are equal.

In an inhomogeneous dielectric medium (air substrate) with unequal phase velocities v_{0e} and v_{0o} when $f_{0e} \neq f_{0o}$, the image impedance Z_c of a lattice section becomes real in a frequency region $\Delta f_c = |f_a - f_b| > 0$ with boundary frequencies f_{0e} and f_{0o} , and the reactances X_a and X_b have different signs in this region. As a result, the all-stop filter circuit represented by the lattice section transforms to the bandpass-filter section under the condition of unequal phase velocities. This

means that the unequal phase velocities of the even- and odd-mode waves in an inhomogeneous dielectric medium cause a change in the frequency characteristic of the filter section.

The attenuation A_p of a lossless, fully balanced bridge-type circuit (in decibels) is defined as

$$A_p = 10 \log_{10} |S_{21}|^{-2} = 10 \log_{10} \left[1 + \frac{(1 + \hat{X}_a \hat{X}_b)^2}{(\hat{X}_a - \hat{X}_b)^2} \right], \quad (8)$$

where S_{21} is the insertion loss of the equivalent two-port network and $\hat{X}_{a,b}$ are the corresponding reactances normalized to the load impedance. From (8), when the frequency of the real image impedances degenerates to $f_a = f_b = f_\infty$, the balanced condition of the partial two-terminal impedances $Z_a(f_\infty) = Z_b(f_\infty)$ is satisfied with the attenuation pole at this frequency. In this case, the greater the values of K_L and K_C , the closer the attenuation pole is to the filter passband.

Note that the ratios of the even- and odd-mode phase velocities v_{0e}/v_{0o} and the ratios of the coefficients of magnetic and electrical couplings K_L/K_C insignificantly depend on the width W and spacing S of two coupled microstrip lines in a homogeneous system. Consequently, the passband bandwidth of the microstrip filter can be changed within very narrow limits. It is important in this case to investigate the ability to control the filter passband bandwidth. Considering the character of voltage and current distribution in a quarter-wave lattice section, it is possible to distinguish two regions with dominant magnetic M and electrical C couplings in its structure [Figure 4(a)]. Such a spatial separation of these types of couplings leads to a simple passband control of the lattice filter section.

In this case, the passband can be extended by increasing the ratio of the magnetic and electrical couplings when $K_L > K_C$ to provide the attenuation pole at frequencies below the passband at the frequency axis. This can be achieved, for example, by reducing the electrical coupling at the ends of the open-circuit lattice section [Figure 4(b)] when the condition $f_\infty < f_b < f_a$ is satisfied. Reducing the magnetic coupling by increasing the length l_0 of the noninteracting line segments [Figure 4(c)] results in a bandwidth narrowing. A further increase of the length l_0 of noninteracting line segments will balance the electromagnetic coupling, and the passband degenerates with $f_a = f_b = f_\infty$. However, for much longer length l_0 when the condition $f_a < f_b < f_\infty$ is satisfied, the electrical coupling dominates and provides the attenuation pole of the lattice filter section at frequencies above the passband. Thus, both the characteristic passband $\Delta f_c = |f_a - f_b|$ and the location of the attenuation poles relative to the characteristic passband can be effectively controlled by varying the coefficients of the electrical and magnetic couplings along the length of the lattice filter section.

T-type, open-stub microstrip sections operating as impedance transformers can also represent the stop-band filter sections with the attenuation poles at higher frequencies. However, in a compact implementation of both T-type and lattice sections in the structure of a microstrip filter, the undesired electromagnetic coupling between them becomes stronger, resulting in degeneration of the attenuation poles formed by each of these filter sections. Note that, in a multicoupled microstrip filter structure, the most prominent attenuation poles can be created only after they have been split, and any superposition or interleaving of the attenuation poles leads to their partial or full degeneration.

Figure 5(a) shows the two-resonator microstrip filter structure with a combination of the T-type and lattice

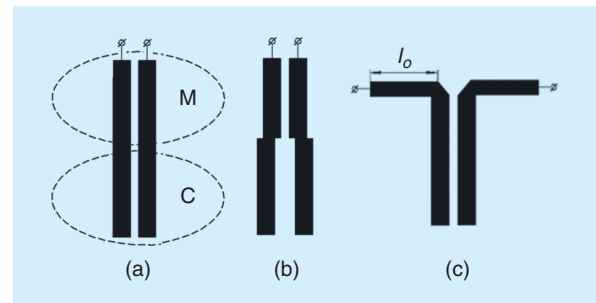


Figure 4. The structures of a lattice section with unequal phase velocities. (a) A structure with two regions having dominant magnetic M and electrical C couplings. (b) A structure with reduced electrical coupling at the ends of the open-circuit lattice section when the condition $f_\infty < f_b < f_a$ is satisfied. (c) A structure having reduced magnetic coupling by increasing the length l_0 of the noninteracting line segments, resulting in a narrowing of bandwidth.

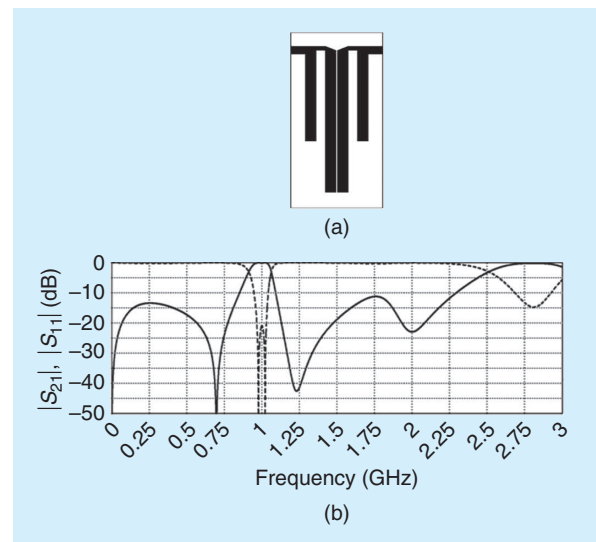


Figure 5. (a) The structure of a two-resonator microstrip filter. (b) A graph showing its insertion and return loss response.

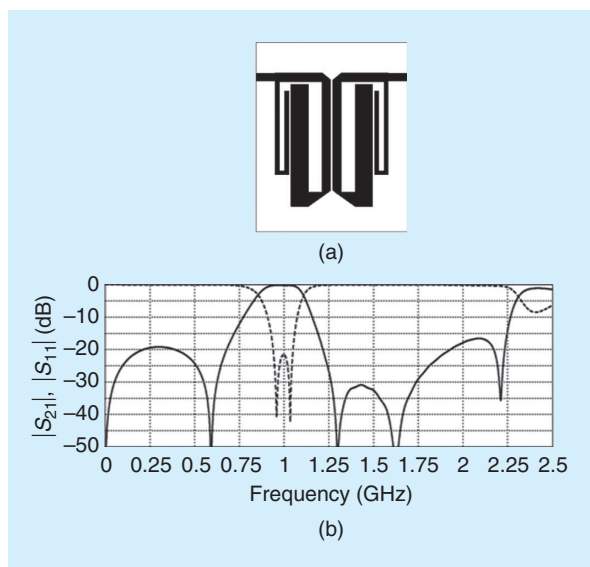


Figure 6. (a) The structure of a microstrip filter with dominant electrical coupling. (b) A graph showing its insertion and return loss response.

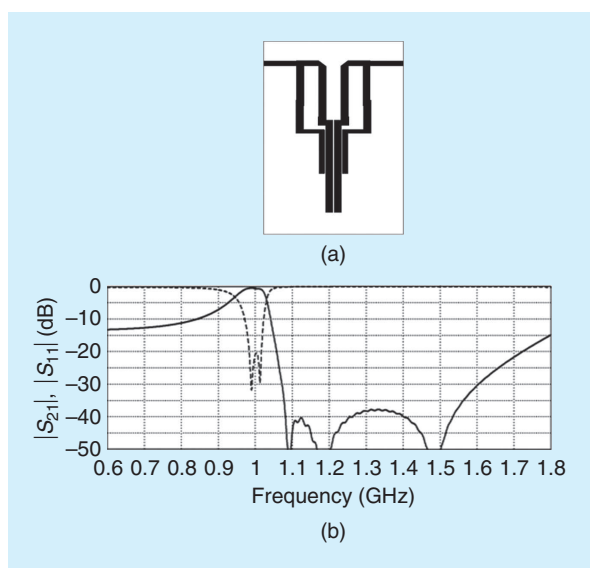


Figure 7. (a) The structure of a microstrip filter with improved single-side selectivity. (b) A graph showing its insertion and return loss response.

sections, where the degeneration is seen with accurate electromagnetic 3D simulations [Figure 5(b)] using a ceramic substrate with effective dielectric permittivity $\epsilon_r = 10.6$ and thickness $H = 1.27$ mm, a distance between the substrate and top cover of 5 mm, and minimal spacing between adjacent microstrip lines $S = 0.15$ mm. As seen in Figure 5(b), the attenuation pole of a quarter-wave lattice section with dominant magnetic coupling between the microstrip lines is formed below the passband. The attenuation poles of the T-type, open-stub microstrip sections formed at

higher frequencies above the passband have degenerated, which is the result of electromagnetic coupling between these T-type and lattice microstrip sections. Note that the dominant coupling between these elements is magnetic coupling when $K_L > K_C$ due to the microstrip structure where $v_{0e} < v_{0o}$.

To provide the dominant electrical coupling between two resonators, 180° bended half-wave resonators can be used. Figure 6(a) shows the structure of a two-resonator microstrip filter with dominant electrical coupling between the branches of each half-wave resonator and its insertion and return loss response of up to 2.5 GHz, shown in Figure 6(b). In this compact structure, the four $(N + 2)$ split attenuation poles at certain frequencies are created, where the first and fourth attenuation poles are formed by the lattice filter section while the second and third are formed by the folded T-type, open-stub microstrip sections.

To form the attenuation poles at frequencies above the passband with dominant electrical coupling, the lattice section in a two-resonator microstrip filter structure should be a quarter wavelength [Figure 7(a)]. The filter insertion and return loss response is shown in Figure 7(b), where the splitting of the attenuation poles formed by the T-type, open-stub microstrip sections is achieved by strengthening the electrical coupling between branches of each resonator at their ends. In such a structure, the electrical coupling is dominant between all microstrip lines.

Castling of Attenuation Poles

One method to redistribute the attenuation poles is called *castling*. Here, the attenuation poles formed by the T-type, open-stub microstrip sections should be located at frequencies below the passband, while the attenuation pole formed by the lattice filter section should be shifted to frequencies above the passband. This can be explained because both T-type and lattice sections contain series microstrip-line sections, l_0 for the lattice section shown in Figures 2(c) and 4(c) and l_ϕ with electrical length θ_ϕ for the T-type section shown in Figures 2(d) and 8(a), which are connected within the common filter structure. Physically, both microstrip lines have positive electrical lengths when considered separately. Theoretically, each length can be negative, taking into account that the overall length is positive and physically realizable, i.e., $l_0 + l_\phi > 0$. For example, assuming that θ_ϕ is negative, then the attenuation pole in such a hypothetical T-type impedance inverter will be formed below the passband, i.e., the position of the attenuation pole changes relative to the passband. In this case, the negative length l_ϕ is compensated for by the positive length l_0 of the lattice section, with overall positive length to be physically realizable.

Let us now define the conditions under which implementation of such a distribution of the attenuation

poles becomes possible. Because each T-type open-stub microstrip section represents a symmetrical circuit, an equivalent, fully balanced bridge-type circuit can be obtained by using the method of mirror images [Figure 8(a)]. Figure 8(b) shows the frequency dependences of the corresponding two-terminal reactances X_a and X_b of such an equivalent circuit for the physically realistic case when the electrical length θ_φ of the microstrip line of length l_φ is positive. At the same time, Figure 8(c) shows the frequency dependences of the corresponding two-terminal reactances X_a and X_b for the case when $\theta_\varphi < 0$.

From an analysis of these reactance dependences, the following conclusions can be drawn.

- 1) For a traditional T-type, open-stub microstrip section with $\theta_\varphi > 0$, the stopbands (frequency bandwidths where the reactances X_a and X_b have different signs in this region, positive for X_a and negative for X_b) and passbands (frequency bandwidths where the reactances X_a and X_b have the same signs in this region, negative for both X_a and X_b) alternate, thus providing a band-stop filter performance with the second attenuation pole between the third and fourth harmonics and $X_a(f_\infty) = X_b(f_\infty)$.
- 2) For a hypothetical T-type, open-stub microstrip section with $\theta_\varphi < 0$, the passbands and stopbands alternate, thus providing a band-pass filter performance with the first attenuation pole at frequencies below the passband and the second additional attenuation pole between the second and third harmonics, which is sufficiently close to the passband.

From the circuit theory for high-order microwave circuits, the problem of negative electrical lengths of transmission lines can be easily eliminated when they can be fully absorbed by the positive lengths of the other transmission lines [14]. In the proposed structure, the negative electrical length θ_φ of the microstrip line of length l_φ can be absorbed by the positive electrical length θ_0 of the microstrip line of length l_0 of the lattice structure. As a result, $\theta_\varphi + \theta_0 > 0$, and the entire filter structure becomes physically realizable and very compact.

Such a distribution of the passbands and stopbands of the constituent sections of a two-resonator filter on the frequency axis determines its substantially higher selectivity properties. Figure 9(a) shows the structure of a two-resonator microstrip filter with castling of the attenuation poles, where two attenuation poles are formed at frequencies below the passband by the T-type, open-stub microstrip section (poles ① and ②). Splitting of the attenuation poles is provided by the dominant magnetic (not electrical) coupling between each branch of the half-wave resonators, with the filter insertion and return loss response shown in Figure 9(b). The minimal spacing between the adjacent microstrip

lines of $S_{\min} = 0.15$ mm enables the realization of a filter structure using any existing substrate technology process. The maximal and minimal widths of the microstrip lines are equal to $W_{\max} = 1.8$ mm and $W_{\min} = 0.6$ mm, respectively. At the same time, five attenuation poles are created at frequencies above the passband, thus contributing to a spectrum free of undesired parasitic passbands. In this case, the first two poles, which are close to the passband (poles ③ and ④), are formed by the lattice section, and the other split auxiliary attenuation poles are formed by the T-type, open-stub microstrip sections [Figure 8(c)] in the frequency range corresponding to the second harmonic. The total number of attenuation poles formed in such a multicoupled compact two-resonator structure is equal to $N + 5$, which determines the improved frequency selectivity of this structure due to castling of the attenuation poles

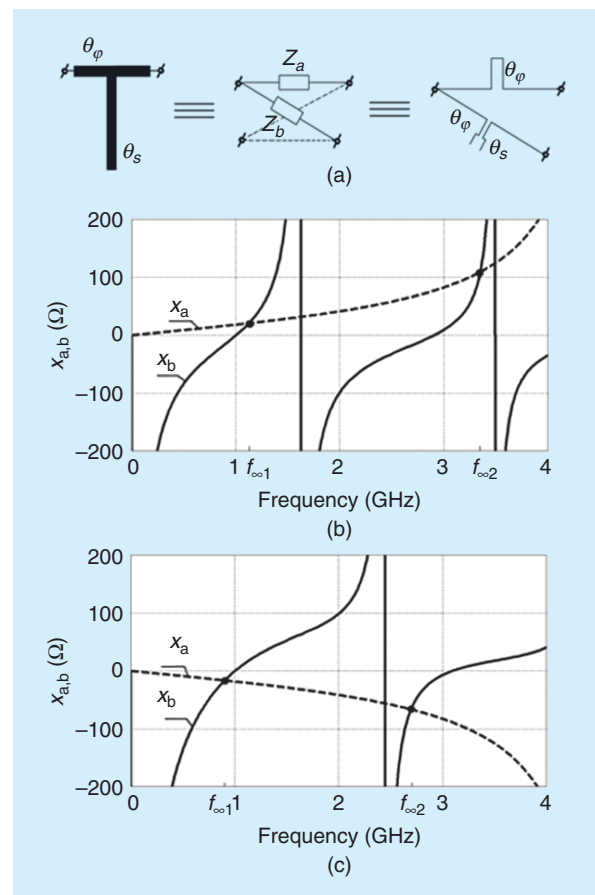


Figure 8. (a) An equivalent, fully balanced bridge-type circuit for a T-type, open-stub microstrip structure. (b) A graph showing the frequency dependences of the corresponding two-terminal reactances X_a and X_b of such an equivalent circuit for the physically realistic case when the electrical length θ_φ of the microstrip line of length l_φ is positive. (c) A graph showing the frequency dependences of the corresponding two-terminal reactances X_a and X_b for the case when $\theta_\varphi < 0$.

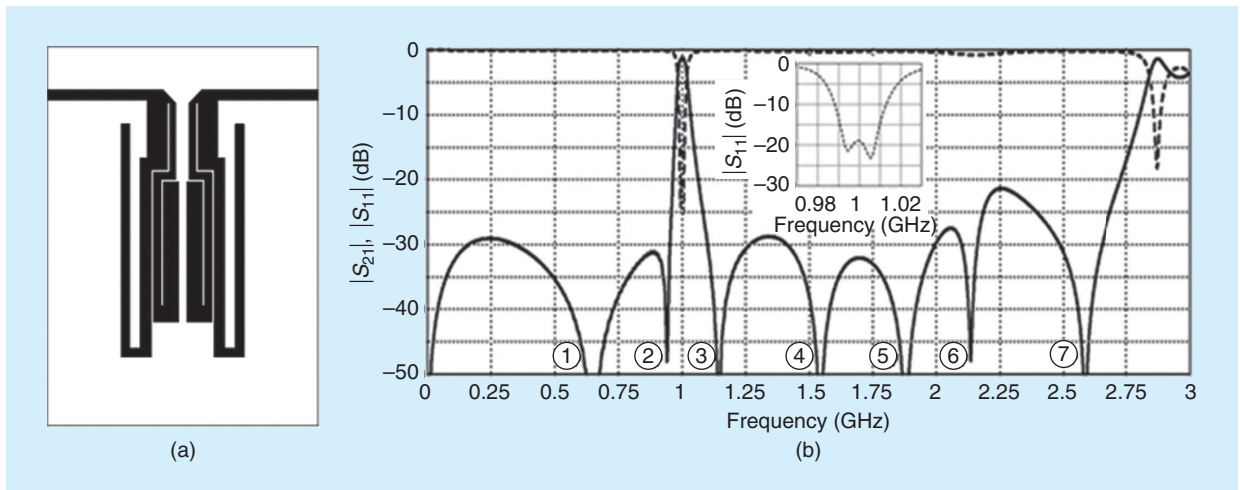


Figure 9. (a) The structure of a two-resonator microstrip filter with castling of attenuation poles. (b) A graph showing its insertion and return loss response.

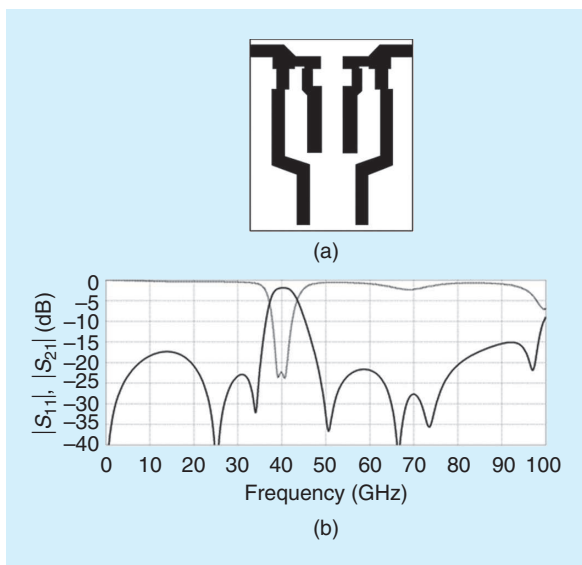


Figure 10. (a) The structure of a two-resonator microstrip filter with additional coupling between its branches. (b) A graph showing its insertion and return loss response.

when compared to Figures 6 and 9. The substrate size for the entire filter structure shown in Figure 9(a) is $11.2 \times 23.0 \text{ mm}^2$ or $0.02\lambda^2$, where λ is the length of the quasi-T wave.

Figure 10(a) shows the structure of a two-resonator microstrip filter with additional coupling between its branches. The insertion and return loss response of this structure [Figure 10(b)] results from electromagnetic 3D simulation of the two-resonator microstrip filter with a central passband frequency $f_0 = 40 \text{ GHz}$ implemented on a ceramic substrate with thickness $H = 0.25 \text{ mm}$ and effective dielectric permittivity $\epsilon_r = 8.9$. Here, the size of the substrate is $1.1 \times 1.2 \text{ mm}^2$, with a minimal width of the microstrip lines of $W_{\min} = 60 \mu\text{m}$

and minimal spacing between the adjacent microstrip lines of $S_{\min} = 60 \mu\text{m}$. The weak electromagnetic coupling between two T-type, open-stub microstrip sections defines the level of splitting of the attenuation poles at frequencies below the passband. Note that this operation mode for both two-resonator filter structures shown in Figures 9(a) and 10(a) is caused by the dominant electric or magnetic coupling between the adjacent microstrip lines and is changed when compared with its prototype structure [Figure 6(a)] when the electric coupling between the microstrip-line elements is replaced by the dominant magnetic coupling and vice versa.

The proposed filter structures based on two half-wave codirectional hairpin resonators in this operation mode exhibit the properties of the multiresonant microwave circuits, which can open up new opportunities in the design and development of high-selectivity microstrip bandpass filters using structures with a limited number of resonators.

Four-Resonator Microstrip Filters and Their Practical Implementation

The effectiveness of this approach in designing high-selectivity microstrip bandpass filters with a limited number of resonators can also be demonstrated by comparing the electrical parameters of four-resonator microstrip filter structures on codirectional hairpin resonators with and without castling of the attenuation poles. These filter structures were selected because they could provide substantially more attenuation poles compared to filter structures with additional couplings between nonadjacent resonators, as shown in Figure 1(c).

Figure 11(a) shows the symmetrical structure of a microstrip bandpass filter without castling of the attenuation poles. The filter is composed of three

quarter-wave lattice sections, with dominant magnetic coupling between adjacent microstrip lines in the left- and right-hand sections and dominant electrical coupling between microstrip lines in the central lattice section.

Here, the left- and right-hand lattice sections provide attenuation poles at frequencies below the passband (poles ① and ②), and splitting is the result of a magnetic coupling between these lattice sections [Figure 11(b)]. At the same time, the central lattice section provides the attenuation pole closest to the passband at frequencies above the passband (pole ③). Splitting of the attenuation poles formed by the T-type, open-stub microstrip sections at higher frequencies (poles ④ and ⑤) is achieved by marginal electrical coupling between nonadjacent resonators. When this coupling is absent, the attenuation poles formed by the T-type, open-stub microstrip sections coincide and degenerate. However, when coupling is significant, the attenuation poles split and interleave with the attenuation poles formed by the central lattice section, which also leads to their degeneration. To form the pronounced attenuation poles, it is necessary to distribute them across the frequency axis in a certain way. In a current implementation of the four-resonator microstrip bandpass filter, the corresponding five basic and two additional split attenuation poles at higher frequencies are formed by the left- and right-hand lattice sections in the frequency range corresponding to the second harmonic.

As a practical example, a four-resonator filter structure was implemented on a ceramic substrate with thickness $H = 1.27$ mm, effective dielectric permittivity $\epsilon_r = 10.9$, strip metallization thickness of $17 \mu\text{m}$, and minimal spacing between adjacent microstrip lines of $S_{\text{min}} = 0.2$ mm. The maximal and minimal widths of the microstrip lines are equal to $W_{\text{max}} = 3.45$ mm and $W_{\text{min}} = 0.5$ mm, respectively. Figure 12(a) shows the test board of a four-resonator microstrip filter, with its return and insertion loss response shown in Figure 12(b). The test board is in good agreement with the corresponding simulation results shown in Figure 11(b). In this case, the insertion loss at the central passband frequency is not more than 1.4 dB, and the relative 3-dB passband bandwidth is equal to 13%. The substrate size for the entire filter structure [Figure 11(a)] is $0.045\lambda^2$, which is only twice as large as the filter structure shown in Figure 9(a).

The number of attenuation poles in a four-resonator structure can be increased by applying the castling approach. Figure 13(a) shows a helicopter-like structure of a three-resonator microstrip bandpass filter based on codirectional hairpin resonators supplemented by a fourth half-wave resonator connected in parallel to a central resonator of the original structure. This supplementary resonator forms two additional attenuation

poles (poles ③ and ④) located near the passband at the left- and right-hand sides [Figure 13(b)]. The symmetry of these attenuation poles relative to the passband is provided by the corresponding selection of the electrical and magnetic couplings between the branches of the supplementary resonator. The T-type, open-stub microstrip sections create the basic attenuation pole at frequencies below the passband (poles ① and ②), and their splitting level is provided using a magnetic coupling between the branches of the left- and right-hand resonators of this structure. The partial compensation for this magnetic coupling is achieved by the electrical

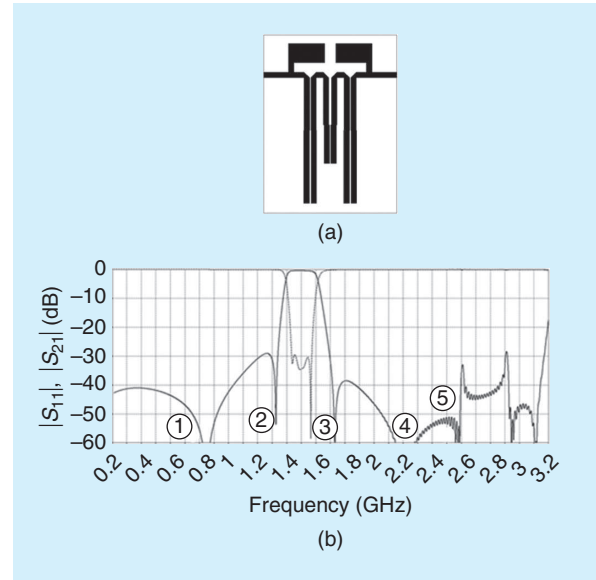


Figure 11. (a) The structure of a four-resonator microstrip filter. (b) A graph showing its quasisymmetrical amplitude response.

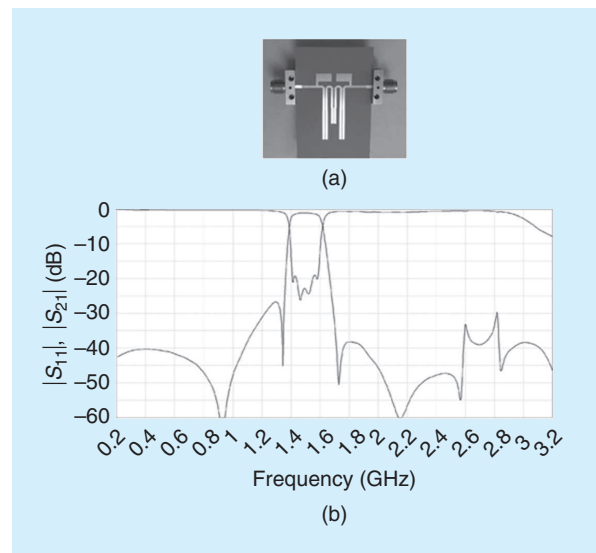


Figure 12. (a) The test board of a four-resonator microstrip filter. (b) A graph showing its return and insertion loss response.

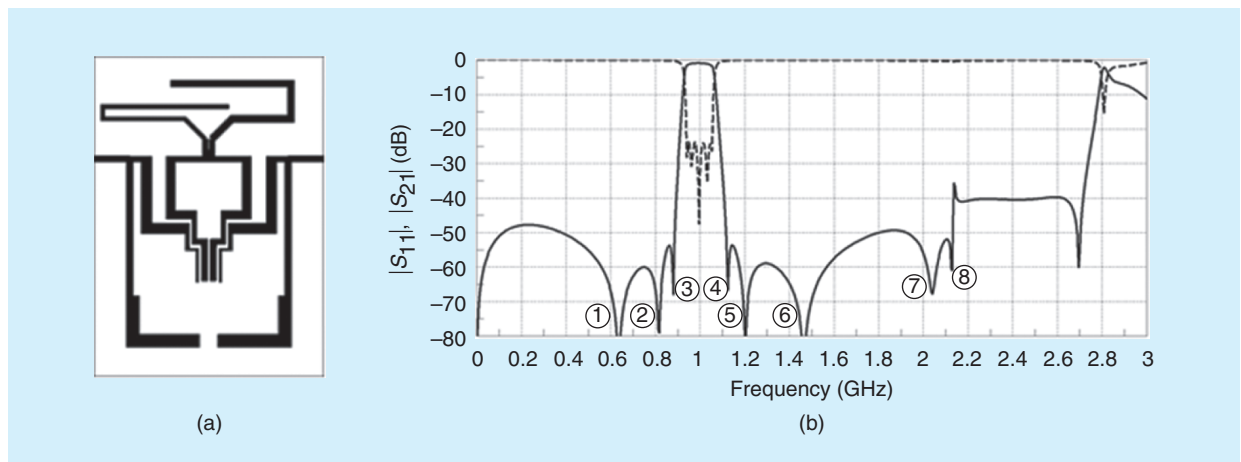


Figure 13. (a) The helicopter-like structure of a four-resonator microstrip filter. (b) A graph showing its insertion and return loss response.

coupling between two open-circuit stubs, and this weak electrical coupling contributes to the splitting of the attenuation poles (poles ⑦ and ⑧) formed by the T-type, open-stub microstrip sections at frequencies above the passband in the range corresponding to the second harmonic, according to Figure 8(c).

Both lattice sections with dominant electrical coupling between the microstrip lines create attenuation poles (poles ⑤ and ⑥) at high frequencies as well, when splitting of the attenuation poles is achieved by electrical coupling between the branches of the central resonator. Here, the minimal spacing between the coupled microstrip lines is $S_{\min} = 0.1$ mm, which can be easily realized using any thin-film technology. The minimum and maximum widths of the microstrip lines are equal to $W_{\min} = 0.5$ mm and $W_{\max} = 1.82$ mm, respectively. The total number of the created attenuation poles in a helicopter-like, four-resonant structure of the microstrip bandpass filter is equal to 9, i.e., $2N + 1$, and the number of the attenuation zeros is equal to $N + 1$. In this case, the roll-off factor, defined as the ratio of filter passbands at the attenuation levels of -40 and -3 dB, respectively, is equal to 1.67. The substrate size for the entire filter structure shown in Figure 13(a) is $0.085\lambda^2$. For comparison, the substrate size of the microstrip filter structure based on four hairpin resonators with additional electromagnetic coupling between nonadjacent resonators [Figure 1(c)] is $0.0625 \lambda^2$ [9]. Note that only two attenuation poles are formed in this four-hairpin resonator structure, similar to the resonator-embedded, four-pole, cross-coupled filter structure [15].

The proposed helicopter-like, four-resonator microstrip bandpass filter shown in Figure 13(a) exhibits an insertion loss more than two times lower with more attenuation poles, a higher roll-off factor, and a more compact structure than that of a four-resonator microstrip bandpass filter based on the parallel-

coupled quarter-wave microstrip lines and a six-order hairpin bandpass filter [16]. At the same time, having a similar level of insertion loss across the passband and out-of-band spurious suppression, the helicopter-like, four-resonator microstrip bandpass filter based on the castling approach offers a significantly steeper roll-off factor and a much smaller size compared to the parallel-coupled microstrip bandpass filter based on the four-stage, stepped-impedance-coupled resonator [17].

The comparative analysis of the proposed four-resonator structures shows that, under the same conditions, a microstrip bandpass filter with castling of the attenuation poles provides both a steeper roll-off factor of the filter amplitude response and a significantly higher attenuation level of stopbands in a very compact size.

Conclusions

Based on theoretical predictions and accurate 3D electromagnetic simulations, nontraditional microstrip bandpass-filter structures with a substantially limited number of codirectional hairpin resonators can create a significant number of attenuation poles at certain frequencies, often exceeding the number of resonators in a filter structure. This will provide much higher frequency selectivity of the microstrip bandpass filter by combining the effects of using different wave properties of the microstrip lines and particular design methods to control the wave processes in them. These methods are based on 1) an effect of the normal waves' nonequal phase velocities, corresponding to even and odd operation modes in a system of coupled microstrip lines; 2) setting the certain degree of the magnetic and electrical couplings at sections of different lengths, between both adjacent microstrip lines and nonadjacent resonators; and 3) using a castling approach for the attenuation poles. It is important during the design procedure to pay close attention to the distribution of attenuation

poles along the frequency axis because their superposition or interleaving can result in degeneration.

Acknowledgments

We thank Dr. Vladimir Chernyshev for his valuable comments and useful discussions.

References

- [1] E. G. Cristal and S. Frankel, "Hairpin-line and hybrid hairpin-line/half-wave parallel-coupled-line filters," *IEEE Trans. Microw. Theory Techn.*, vol. MTT-20, pp. 719–728, Nov. 1972.
- [2] J. D. Rhodes, *Theory of Electrical Filters*. New York: Wiley, 1976.
- [3] M. I. Lancaster and J. S. Hong, "Theory and experiment of novel microstrip slow-wave open-loop resonator filters," *IEEE Trans. Microw. Theory Techn.*, vol. MTT-45, pp. 2358–2365, Dec. 1997.
- [4] J. G. Hong and M. J. Lancaster, *Microstrip Filters for RF/Microwave Applications*. New York: Wiley, 2001.
- [5] T. Kitamura, Y. Horii, M. Geshiro, and S. Sawa, "A dual-plane comb-line filter having plural attenuation poles," *IEEE Trans. Microw. Theory Techn.*, vol. MTT-50, pp. 1216–1219, Apr. 2002.
- [6] K. Ma, K. S. Yeo, J. Ma, and M. A. Do, "An ultra-compact hairpin band pass filter with additional zero points," *IEEE Microw. Compon. Lett.*, vol. 17, no. 4, pp. 262–264, Apr. 2007.
- [7] H. P. Partal, "Cross coupled wiggly line hairpin filters with high selectivity and spurious suppression," in *Proc. 40th European Microwave Conf.*, 2010, pp. 1265–1268.
- [8] M. Sanchez-Renedo, R. Gomez-Garcia, and R. Loeches-Sanchez, "Microstrip filters with selectivity improvement using the new concept of signal-interference source/load coupling," in *Proc. 2013 IEEE MTT-S Int. Microwave Symp. Dig.*, pp. 1–4.

- [9] J.-T. Kuo, M.-J. Maa, and P.-H. Lu, "A microstrip elliptic function filter with compact miniaturized hairpin resonators," *IEEE Microw. Guided Wave Lett.*, vol. 10, pp. 94–95, Mar. 2000.
- [10] G. M. Aristarkhov and V. P. Chernyshev, "Indirect synthesis of microstrip filters employing codirectional comb resonators (in Russian)," *J. Commun. Technol. Electron.*, vol. 32, pp. 34–40, Oct. 1987.
- [11] A. Grebennikov, *RF and Microwave Transmitter Design*. Hoboken, NJ: Wiley, 2011.
- [12] G. L. Matthaei, "Narrow-band, fixed-tuned, and tunable band-pass filters with zig-zag hairpin-comb resonators," *IEEE Trans. Microw. Theory Techn.*, vol. MTT-51, pp. 1214–1219, Apr. 2003.
- [13] G. M. Aristarkhov and V. P. Chernyshev, "Equivalent mode representation of microstrip filters using multi-conductor lines with unequal velocities" (in Russian), *J. Commun. Technol. Electron.*, vol. 31, pp. 1–7, Apr. 1986.
- [14] G. L. Matthaei, L. Young, and E. M. T. Jones, *Microwave Filters, Impedance-Matching Networks, and Coupling Structures*. Norwood, MA: Artech House, 1980.
- [15] S. Y. Lee and C. M. Tsai, "New cross-coupled filter design using improved hairpin resonators," *IEEE Trans. Microw. Theory Techn.*, vol. MTT-48, pp. 2482–2490, Dec. 2000.
- [16] S. Zhang and L. Zhu, "Synthesis method for even-order symmetrical Chebyshev bandpass filters with alternative J/K inverters and $\lambda/4$ resonators," *IEEE Trans. Microw. Theory Techn.*, vol. MTT-61, pp. 808–816, Feb. 2013.
- [17] A. Worapishet, K. Srisathit, and W. Surakamponorn, "Stepped-impedance coupled resonators for implementation of parallel coupled microstrip filters with spurious band suppression," *IEEE Trans. Microw. Theory Techn.*, vol. MTT-60, pp. 1540–1548, June 2012.



IEEE Foundation
REALIZE
THE FULL POTENTIAL OF IEEE

ILLUMINATE EDUCATE ENGAGE ENERGIZE

The world's most daunting challenges require innovations in engineering, and IEEE is committed to finding the solutions.

The IEEE Foundation is leading a special campaign to raise awareness, create partnerships, and generate financial resources needed to combat these global challenges.

Our goal is to raise \$30 million by 2020.

DONATE NOW
ieeefoundation.org

